ARTICLE

Application of topographic elevation data generated by remote sensing approaches to flood inundation analysis model

Maulana Ibrahim Rau[1] · Atriyon Julzarika[2] · Natsuki Yoshikawa[3] · Takanori Nagano[4] · Masaomi Kimura[5] · Budi Indra Setiawan[6] · Lan Thanh Ha[7]

Abstract

High-resolution topographic data are crucial for delta water management, such as hydrological modeling, inland flood routing, etc. Nevertheless, the availability of high-resolution topographic data is often lacking, particularly in low-lying regions in developing countries. This data scarcity poses a significant obstacle to inland flood modeling. However, collecting detailed topographic data is demanding, time-consuming, and costly, making remote sensing techniques a promising solution for developing flood inundation analysis models worldwide. This study presents a novel understanding for utilizing topographical elevations obtained using remote sensing techniques to create a flood inundation analysis model. In a study of three watersheds, Kameda, Niitsu, and Shirone (Japan), the assessment of digital terrain models (DTMs) showed that remote sensing-based DTMs (RS-DTMs) exhibited high reliability of coefficient of determination (R^2) and root-mean-square errors, compared with the airborne LiDAR-based topography from the Geospatial Information Authority of Japan. Comparing the flood modeling results from LiDAR data and RS-DTM, with Kameda and Niitsu performing favorable outcomes, Shirone exhibited less accurate results. We hypothesized that this was caused by the topographic distortions due to lack of evenly distributed reference points. Hence, we revised the topography by adjusting both the slope and intercept from the regression equation. This verification successfully showed that the flood inundation volume correlation improved, achieving R^2 results for the three watersheds ranging from 0.975 to 0.997 and Nash–Sutcliffe Efficiencies ranging from 0.938 to 0.986 between the resulting flood models based on the LiDAR data and RS-DTM. Based on these findings, we recognized the significance of uniformly distributed geodetic height points. In areas lacking height references, high-precision survey instruments can be employed for achieving uniform distribution.

Keywords DTM · Topography · Remote sensing · Flood inundation model

✉ Natsuki Yoshikawa
natsuky@agr.niigata-u.ac.jp

1 Graduate School of Science and Technology, Niigata University, 8050 Ikarashi 2-nocho, Nishi-ku, Niigata 950-2181, Japan

2 Research Organization for Earth and Maritime, National Research and Innovation Agency (BRIN), Cibinong, West Java 16915, Indonesia

3 Institute of Science and Technology, Niigata University, 8050 Ikarashi 2-nocho, Nishi-ku, Niigata 950-2181, Japan

4 Graduate School of Agricultural Science, Kobe University, Rokkodai-cho, Nada-ku, Kobe, Hyogo Prefecture 657-8501, Japan

5 Faculty of Agriculture, Kindai University, Nakamachi, Nara, Nara Prefecture 631-0052, Japan

6 Department of Civil and Environmental Engineering, Faculty of Agricultural Technology, IPB University, Bogor, West Java 16680, Indonesia

7 Institute of Water Resources Planning, Ministry of Agriculture and Rural Development, Hanoi 100000, Vietnam

Introduction

Spatial technology is an emerging approach that incorporates geographic information using remote sensing (RS), geographic information systems (GIS), and other instruments and devices (Wilson 2012). These techniques can provide digital elevation models (DEMs), that is, computer representations of elevation using a two-dimensional (*x*–*y* value) array of data containing height information as *z* values (Burrough & McDonnell 1998). A DEM comprises both a digital terrain model (DTM), representing the bare Earth's surface, and a digital surface model (DSM) that captures the Earth's surface, including aboveground features, such as buildings and vegetation. The representations of the *x*, *y*, and *z* values are shown as topographic (overland terrain) and bathymetric (underwater terrain) data. Topographic and bathymetric data have been utilized in many disciplines, such as geomorphology (Guth 2003; Stock et al. 2002), urban studies (Gamba et al. 2002), flood inundation modeling (Ettritch et al. 2018; Chen et al. 2018; Meesuk et al. 2015; Merkuryeva et al. 2015; Rau et al. 2021), and flood analyses of lowland areas (Yoshikawa et al. 2011; Kimura et al. 2019; Nguyen et al. 2020).

The availability of high-resolution topographic data is crucial for various geospatial applications, including flood modeling. However, obtaining accurate topographic information remains a challenge, particularly in lowland areas, where minimal height differences make reliable measurements difficult. Collecting detailed topographic data can be demanding and time-consuming, requiring extensive effort and specialized equipment, such as unmanned aircraft vehicles (UAVs), airborne surveys, light detection and ranging (LiDAR) technology, or terrestrial mapping techniques (involving electronic total stations or global navigation satellite system (GNSS)). Moreover, the high costs associated with these approaches pose significant challenges.

Inundation flood modeling plays a vital role in assessing and managing flood risks in lowland/delta areas. Accurate and reliable flood modeling requires detailed topographic data, enabling precise mapping of the terrain and identification of flood-prone areas. High-resolution DTMs are essential to predict the extent and depth of flood inundation, as demonstrated by Escobar–Silva et al. (2023). This is attainable with the use of airborne LiDAR to penetrate vegetation and accurately capture ground surface information, even in densely vegetated areas. Therefore, LiDAR is commonly used as an accurate data source in various geospatial studies (Lefsky et al. 2002), including flood modeling and assessment (Wedajo 2017). However, applying flood inundation models worldwide presents various challenges, particularly in developing countries with limited access to detailed elevation data (Mesa–Mingorance & Ariza–López 2020).

While the importance of combining flood models with remote sensing has been discussed in previous studies (Néelz et al. 2006; Xu et al. 2021; Jiang et al. 2022), and correction techniques for digital elevation models (DEMs) using remote sensing data have also been introduced (Pavlova and Pavlova 2018; Magruder et al. 2021), the creation of a remote sensing-derived DTM specifically designed for flood modeling remains unaddressed. Therefore, in this study, we assessed the applicability of topographic elevations generated by remote sensing approaches or a remote sensing-based DTM (RS-DTM) to develop a flood inundation analysis model. This study aimed to quantify the performance of the DTM based on comparisons with available high-resolution data in Japan. This study discusses the data acquisition, processing, and verification of a flood inundation analysis model using topographic elevations generated by remote sensing techniques. The approach is expected to be further employed for the application in developing countries and worldwide.

Materials and methods

RS-DTM establishment

To establish the remote sensing-based topography in this study, we integrated satellite imagery from various sources. This dataset served as the primary DTM (DTM master) and was subsequently updated with the latest vertical deformation data (Julzarika 2021) (Fig. 1). The DTM master acted as the central reference point for deriving the RS-DTM (Julzarika et al. 2021a). The initial step in obtaining the DTM master involved DSM extraction, which was customized to the specific input data type used, including satellite imagery, UAV, aerial images, synthetic aperture radar (SAR) (Rucci et al. 2012), stereo imaging, interferometry, LiDAR, videogrammetry, terrestrial surveys, or other mapping sensor varieties. The vertical accuracy and precision of the DSM were directly influenced by the quality of the input data (Julzarika et al. 2021b; Julzarika & Harintaka 2019), leading to the utilization of various DSM extraction methods tailored to different input data types.

In this study, a stereo model method was employed for DSM extraction using PlanetScope, WorldView-2, and Sentinel-1 images, gathered from specific acquisition dates with different spatial resolutions (Table 1). PlanetScope comprises eight multispectral bands, whereas WorldView-2 comprises three or eight bands. Sentinel-1 is a single-look complex (SLC) level. Two DTMs were generated from the
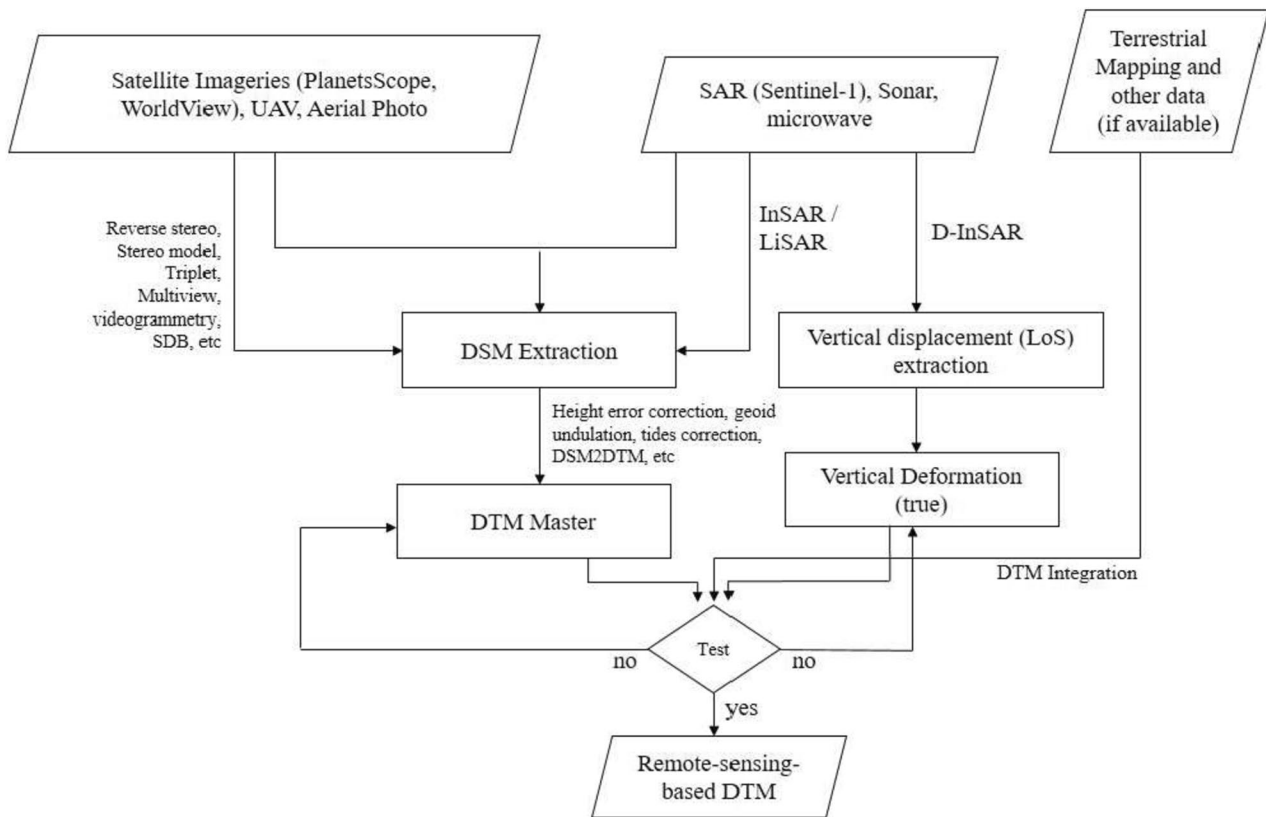
Fig. 1 Remote sensing-based digital terrain model (DTM) establishment

Table 1 Remote sensing data sources and acquisition information for Kameda, Niitsu, and Shirone watersheds

No.	Watershed	Data input	Spatial resolution	Acquisition date	Source	Data availability
1	Kameda	PlanetScope	3 m	30-May-22	Planet Labs PBC	Commercial (free for education and research program)
		WorldView-2	50 cm	12-Nov-22	Maxar Technologies	Commercial
		Sentinel-1	10 m	May-22—Feb-23	European Space Agency and the University of Alaska	Free
2	Niitsu	PlanetScope	3 m	30-May-22	Planet Labs PBC	Commercial (free for education and research program)
		WorldView-2	50 cm	12-Nov-22	Maxar Technologies	Commercial
		Sentinel-1	10 m	May-22—Feb-23	European Space Agency and the University of Alaska	Free
3	Shirone	PlanetScope	3 m	31 October 2022	Planet Labs PBC	Commercial (free for education and research program)
		WorldView-2	50 cm	4 Juni 2020	Maxar Technologies	Commercial
		Sentinel-1	10 m	Oct-22—Nov-22	European Space Agency and the University of Alaska	Free

PlanetScope and WorldView-2 imagery and subsequently integrated to produce the DTM master.

Moreover, vertical deformation information, which included uplift or subsidence, was derived from SAR images using the Differential Interferometric SAR (D-InSAR) method (Julzarika et al. 2021a). The outcome obtained from the application of the D-InSAR technique is represented as the vertical displacement along the line of sight (LoS). To obtain true vertical deformation, it was imperative to correct the LoS measurements. The vertical

displacement, initially represented by the LoS, was subsequently converted into the true vertical deformation (Suhadha et al. 2022), which served as the final output of the RS-DTM.

Afterward, as part of the topography establishment, reference points were used to accurately georeference and align RS-DTM with the local coordinate system (JGD 2011), ensuring precise spatial representation (Bruinsma et al 2012; Jurjević et al 2021). For this study, nine reference points were used, all of which were electronic reference points and first-class control points, obtained from GSI (GSI 2023) and represented with official GSI codes, as shown in Fig. 2. The primary use of elevation data from each point was to establish the height reference for three study watersheds in Niigata Prefecture, Japan. The Kriging method (Hengl et al. 2007) was employed to interpolate elevation values between the nine reference points.

Assessment of RS-DTM

The RS-DTM was assessed using a hydrodynamic flood inundation model (Yoshikawa et al. 2011). In this flood inundation model, the planar analysis domain is represented in topographically adjusted cells (hereafter referred to as "cells"). A cell is an arbitrary polygonal structural grid whose shape can be freely set based on the boundaries of roads, railroads, rivers, and other land use zones that affect flooding phenomena as well as elevation values (Yasuda et al. 2003). Each cell consists of terrain-fitted sides, which serves as boundaries performing as the cells' edges (hereafter referred to as "sides"). These sides encapsulate elevation information within the nodes of the line. Cell formation involves their division into basins, drainage areas, and cells. The shape and arrangement of the cells were varied. In this study, the manual division of cells based on land use was performed. The division of cells was guided by considering obstacles to flood propagation, with the aim of aligning
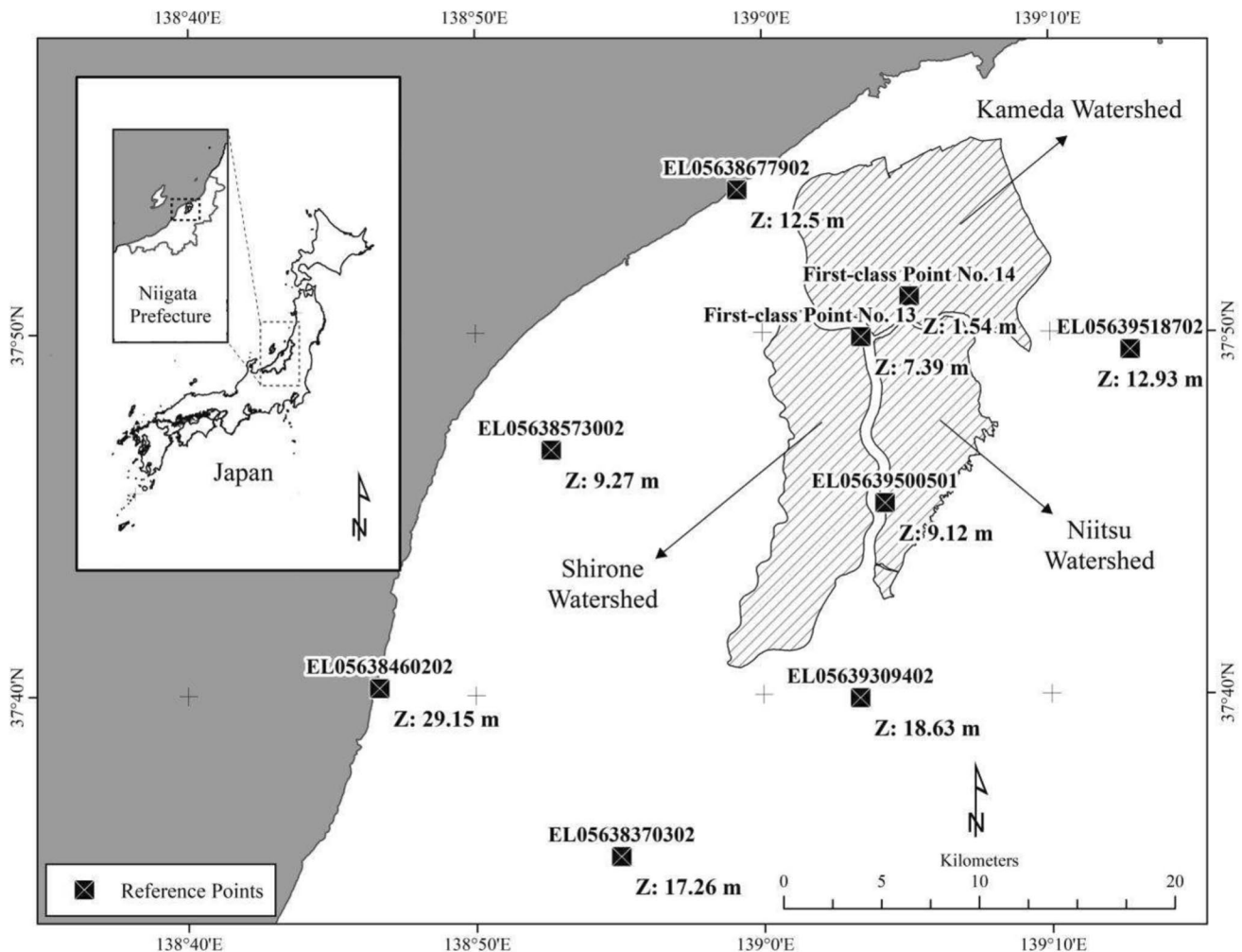

Fig. 2 Reference points used for RS-DTM establishment

the cell edges with natural barriers. The established cells served as fundamental units for conducting flood inundation analyses.

In this study, the applicability of the RS-DTM was verified by comparing it with a validated inundation analysis model constructed using an airborne LiDAR-based DTM with a spatial resolution of 5 m and vertical accuracy of 0.1 m, which was provided by the Geospatial Information Authority of Japan (GSI) (2020). An initial comparison was conducted to determine the most appropriate cell-extraction method. The correlation of cell elevation between the two sources was evaluated using three approaches: centroid, mean, and median. To evaluate the reliability of the DTM, statistical performance indices were used to assess the degree of agreement between simulated and observed values. The two indices used in this study were the coefficient of determination (R^2) and the root-mean-square error (RMSE) (Harel 2009; Van Liew et al. 2003).

Finally, flood inundation analyses were conducted within the three watershed areas, based on previous research. These analyses focused on generating a time series of inundation depth and inundation volume for a 2-day rainfall event within these watersheds. The findings using LiDAR-based DTM from Yoshikawa et al. (2011) were utilized, where the model was subsequently rerun utilizing RS-DTM. In this assessment, the spatial distribution of the flood inundation depth at peak time was compared in addition to the time series variation of the inundation water volume from the two elevation datasets for a rainfall event with a 100-year replication period as the extreme flood event (1% chance of occurrences in any given year). Details of the calculated floodwater volume are provided below.

$$V = \sum_{i=1}^{n} \left(A_i x d_i \right) \qquad (1)$$

where V is the floodwater volume within the watershed, A is the area of the inundated cells, d is the water depth, and n is the total number of calculations based on each cell.

The comparison was then undertaken using two main statistical approaches: the coefficient of determination (R^2) and the Nash–Sutcliffe efficiency (NSE). The NSE is a normalized statistic that determines the relative magnitude of the residual variance ("noise") compared to the measured data variance ("information") (Nash and Sutcliffe 1970).

$$\text{NSE} = 1 - \left[\frac{\sum_{i=1}^{n} \left(Y_i^{\text{obs}} - Y_i^{\text{sim}} \right)^2}{\sum_{i=1}^{n} \left(Y_i^{\text{obs}} - Y^{\text{mean}} \right)^2} \right] \qquad (2)$$

where Y_i^{obs} is the i the observation for the constituent being evaluated, Y_i^{sim} is the i the simulated value for the constituent being evaluated, whereas Y^{mean} is the mean of observed data for the constituent being evaluated, and n is the total number of observations.

Study sites

We selected three watersheds in Niigata Prefecture, namely Kameda (9620 hectares), Niitsu (5120 hectares), and Shirone (7510 hectares) for our study. These areas were specifically chosen due to the existence of previously established flood inundation analysis models established with LiDAR-based DTM data (Table 2). The numbers of cells in the Kameda, Shirone, and Niitsu models were 13,800, 9600, and 20,800, respectively. A common feature of these watersheds is that they are located on an alluvial plain downstream of the Shinano River, the longest river in Japan (367 km), and their topography is extremely flat and low in elevation. Owing to these topographical conditions, drainage pump stations are located at the downstream end of each watershed, and pumps are always in operation to discharge water into the river. This causes flooding problems when rainfall exceeds the pumping capacity.

Results

Topography creation results

RS-DTMs were established for the three watersheds. The generated DTMs for the three areas considered the weight of each input data from PlanetScope, WorldView-2, and Sentinel-1, and the covariance between the parameters used had a spatial resolution of 1 m and a vertical accuracy of < 1 m, satisfying a confidence level of 95% (1.96σ) (Fig. 3). The surface features and cross sections of a sample area within the study area of Kameda are shown in the following visualizations: (a) shows the DTM feature from the LiDAR data, and (b) shows the topography of the RS-DTM within the same area.

Table 2 Topographic characteristics of Kameda, Niitsu, and Shirone watersheds

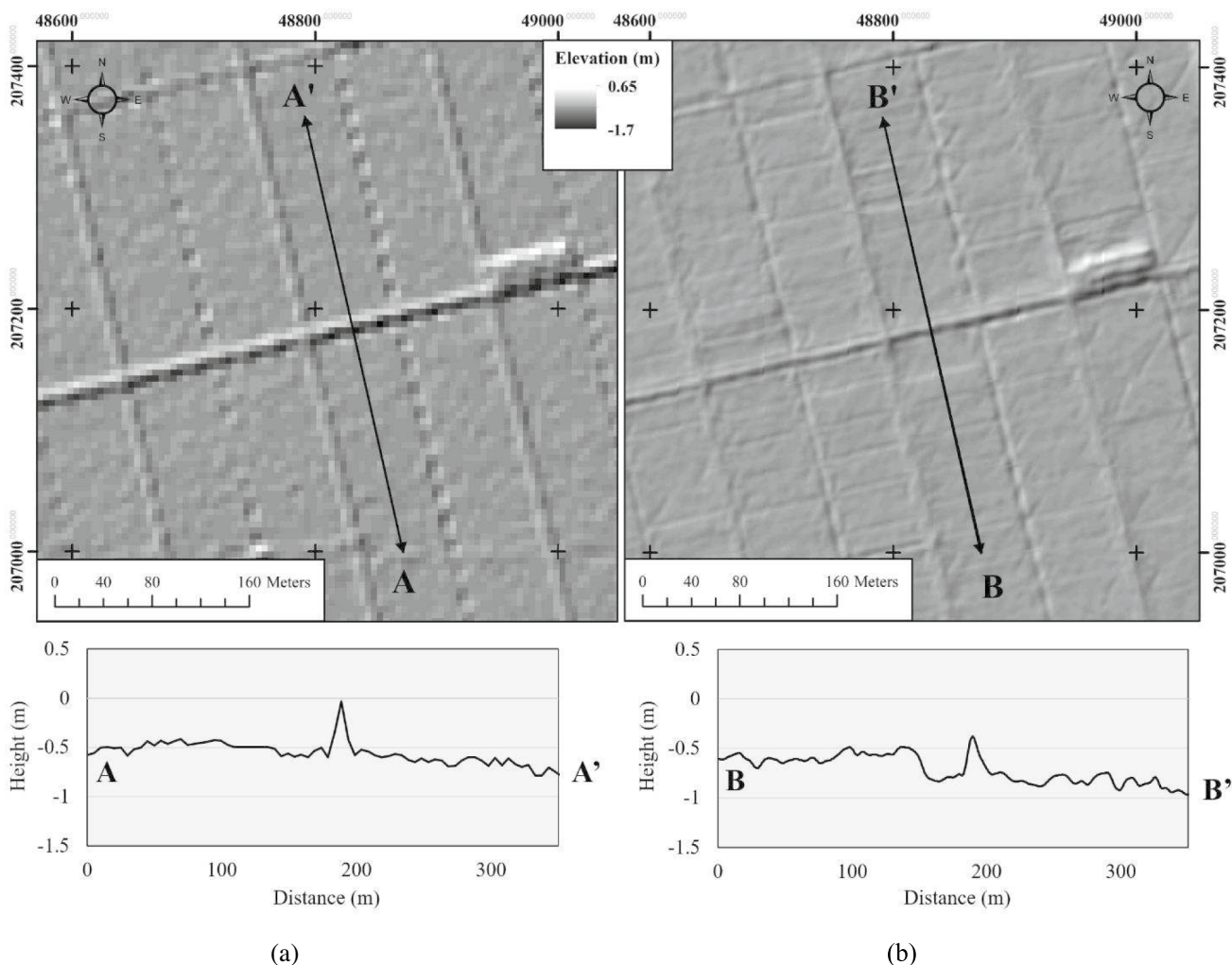| No.	Watershed	Cell size (m²)			Average differences between each cell (m)	Average slope
		Average	Minimum	Maximum		
1	Kameda	6966	65.73	382,745	0.19	1/2990
2	Niitsu	5290	20.45	161,256	0.29	1/4000
3	Shirone	3575	16.80	67,486	0.22	1/2720

Fig. 3 Surface topography of a 5-ha sample area in the Kameda watershed using **a** LiDAR data and **b** self-established remote sensing-based DTM

RS-DTM assessment results

The findings revealed that the R^2 results obtained from centroid, mean, and median approaches had values exceeding 0.93 (Table 3). The median approach was observed to be the most correlated among the other two approaches for the three areas, which is in line with the RMSEs, where the median approach exhibited the smallest errors compared with the other two approaches in all areas. The RMSEs of the three watersheds varied between 0.285 and 0.718 m.

Subsequently, using the median-based approach to determine the representative elevations of individual cells, the average, minimum, maximum, and height difference elevations of the three watershed areas (Table 4) were determined. The results revealed a distinction in the observed patterns among the Kameda, Niitsu, and Shirone watersheds. In particular, the slopes of the regression lines for Kameda and Niitsu watersheds were 1.0005 and

Table 3 Statistical results of comparisons between RS − derived elevation with LiDAR elevation

Approach	Statistical parameters	Study site		
		Kameda	Niitsu	Shirone
Centroid	R^2	0.943	0.956	0.936
	RMSE (m)	0.431	0.718	0.465
Mean	R^2	0.943	0.965	0.966
	RMSE (m)	0.322	0.624	0.404
Median	R^2	0.963	0.994	0.967
	RMSE (m)	0.247	0.234	0.385

0.9931, respectively, which are significantly close to 1, confirming their high reliability. In contrast, Shirone's data exhibited a slope of 0.9431, indicating a slope deviation of approximately 6% (Fig. 4). As for the intercepts of the respective regression lines, the values were 0.061 for the Niitsu, − 0.072 for Kameda, and -0.095 for Shirone, which is

Table 4 Comparisons of elevations using the median-based approach

No.	Watershed	LiDAR elevation (m)			Remote sensing-based elevation (m)		
		Ave.	Min.	Max.	Ave.	Min.	Max.
1	Kameda	1.10	−1.86	11.60	1.20	−1.33	12.12
2	Niitsu	4.18	0.82	58.88	4.41	0.12	58.97
3	Shirone	1.95	−0.73	12.45	1.73	−0.99	11.80
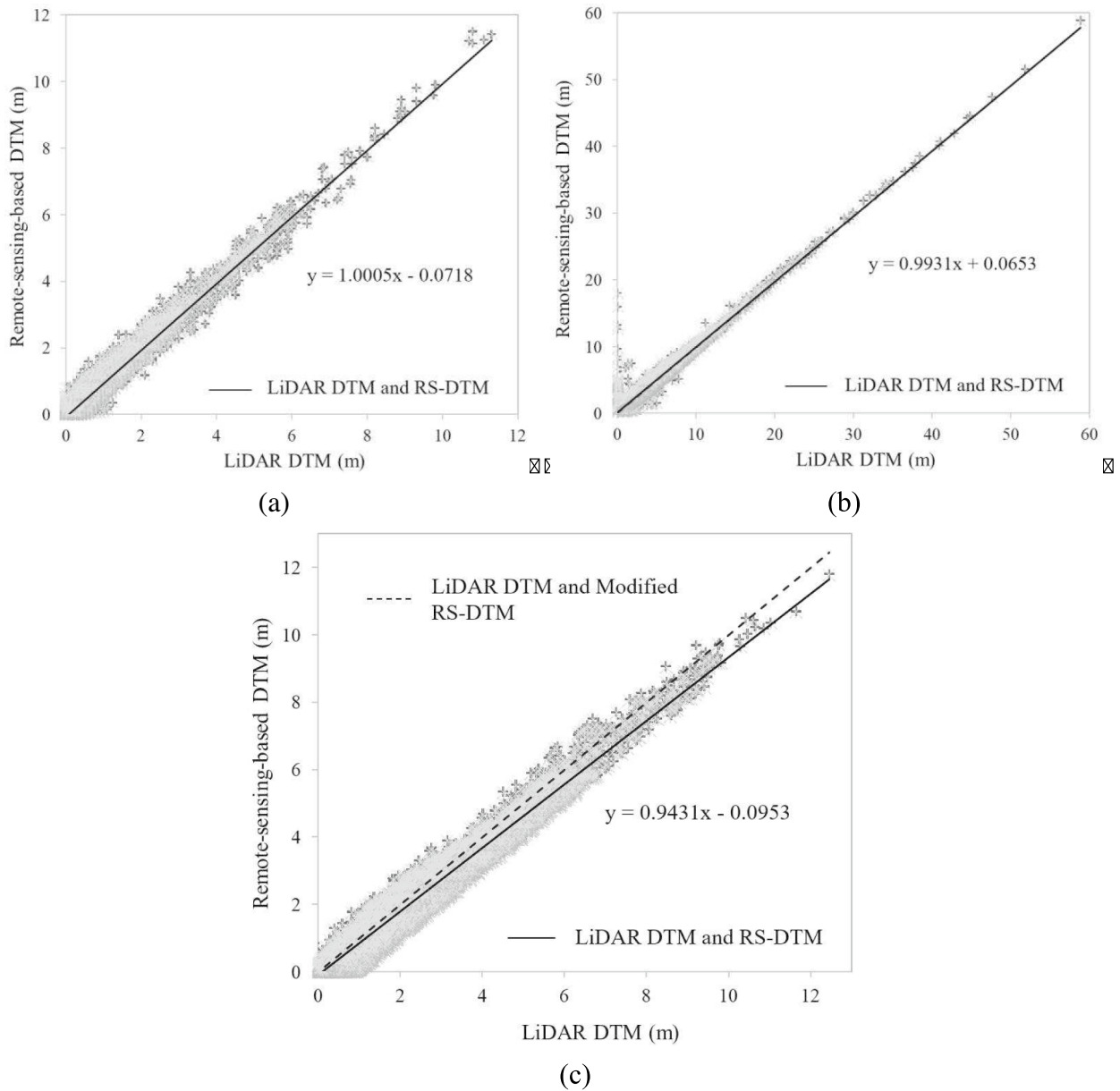
Fig. 4 Comparisons of DTM between LiDAR, remote sensing-based DTM, and modified RS-DTM in **a** Kameda, **b** Niitsu, and **c** Shirone

well within the acceptable range considering that the vertical accuracy of the LiDAR-based DTM is 0.1 m.

Application and modification of RS-DTM for inland flood modeling

Application of RS-DTM's original elevation for inland flood modeling

By applying the constructed RS-DTM to create an inland flood model, the analysis of water volume hydrographs revealed a consistent trend that aligned closely with the curves calculated using LiDAR elevation data (Fig. 5). Notably, the results from the Kameda watershed demonstrated the most promising outcomes, with a peak flood inundation volume difference of 0.07×10^5 m^3. For the Niitsu watershed, the peak water volume difference accounted for 0.95×10^5 m^3, whereas the Shirone watershed exhibited the largest difference reaching 2.05×10^5 m^3.

Furthermore, both Kameda and Niitsu methods showed R^2 and NSE values exceeding 0.9, indicating satisfactory results. In contrast, the Shirone watershed exhibited a weaker correlation than the two watersheds. Although the R^2 value was classified as very good, the NSE yielded in a 'good' category outcome (Table 5). Based on these results, a general approach to overcome less correlated outcomes is necessary.

Topography revision based on intercept and slope from regression analyses

The authors hypothesized that a weaker correlation observed in the Shirone area could be attributed to unevenly distributed reference points. Consequently, we investigated whether better results could be obtained by adjusting both the slope and intercept of the regression equation to correct for topographic distortions due to lack of evenly distributed reference points.

The slope value for Shirone watershed was 0.9431, indicating a roughly 6% deviation, while those of Kameda and Niitsu were close to 1 (Table 6), indicating a near-perfect alignment with the expected slope. The height difference map indicated that greater disparities were observed in regions more distant from the reference points employed, especially in the southern and western parts of Shirone (Fig. 6). Additionally, the map illustrated variations in slope between the LiDAR and RS-DTM, as evaluated along a cross-sectional line within the Shirone Watershed.

Moreover, the revision of topography in our adjustments was also undertaken to the intercept. In such cases, the intercept serves as a crucial reference point for the LiDAR and RS-DTM relationship. However, a near-perfect slope implies that the predictive power of the RS-DTM is intact, and any adjustments to the intercept could potentially introduce unnecessary bias or error. Preserving the original intercept at a near-perfect slope condition ensures stability and accurate representation of both DTM relationships. Conversely, when slopes are deviated, revisions to the intercept may be necessary to align the RS-DTM with the LiDAR data more effectively. Hence, for both Kameda and Niitsu, in addition to the previously mentioned rationale, given the insignificance of intercept errors, we considered that no revisions are required. Consequently, only the Shirone area underwent revision, accomplished by multiplying the elevations by a factor of 1/0.9431 and adding 0.095 m for all elevations.

Based on the inland flood model, the changes involved all related topographic parameters, including both the cells and sides (nodes of each cell).

Revised RS-DTM results

To assess the impact of the topographic revision, the water flood volumes were recalculated by considering the slope obtained from the regression analyses for Shirone watershed (Fig. 5). The results revealed a consistent trend that was more closely aligned with the curves calculated using LiDAR elevation data. In terms of the flood inundation volume difference at peak time, the difference was 1.15×10^5 m^3.

After incorporating the revised topographic elevation data for the Shirone watershed, the statistical performance improved significantly. The R^2 value increased to 0.997, whereas the NSE value reached 0.938, both of which were classified as very good. These findings further support the accuracy and effectiveness of regression models based on topographic elevations for flood modeling applications.

In addition, visual representations in the form of maps were created to depict the flood inundation depth at peak time within each watershed (Fig. 7). These maps provide visualization of the extent of flooding in the study area. The inundation depth was classified into distinct categories: areas with a depth of less than 1 cm were classified as non-inundated, whereas inundated areas were colored using shades of gray. The classifications for inundated areas were further divided into four categories based on water depth: 0.01–0.2 m, 0.2–0.4 m, 0.4–0.6 m, and greater than 0.6 m. The maps reveal variations in inundation depth values, yet consistently show the overall consistencies of inundation representations across the three watersheds in both models.
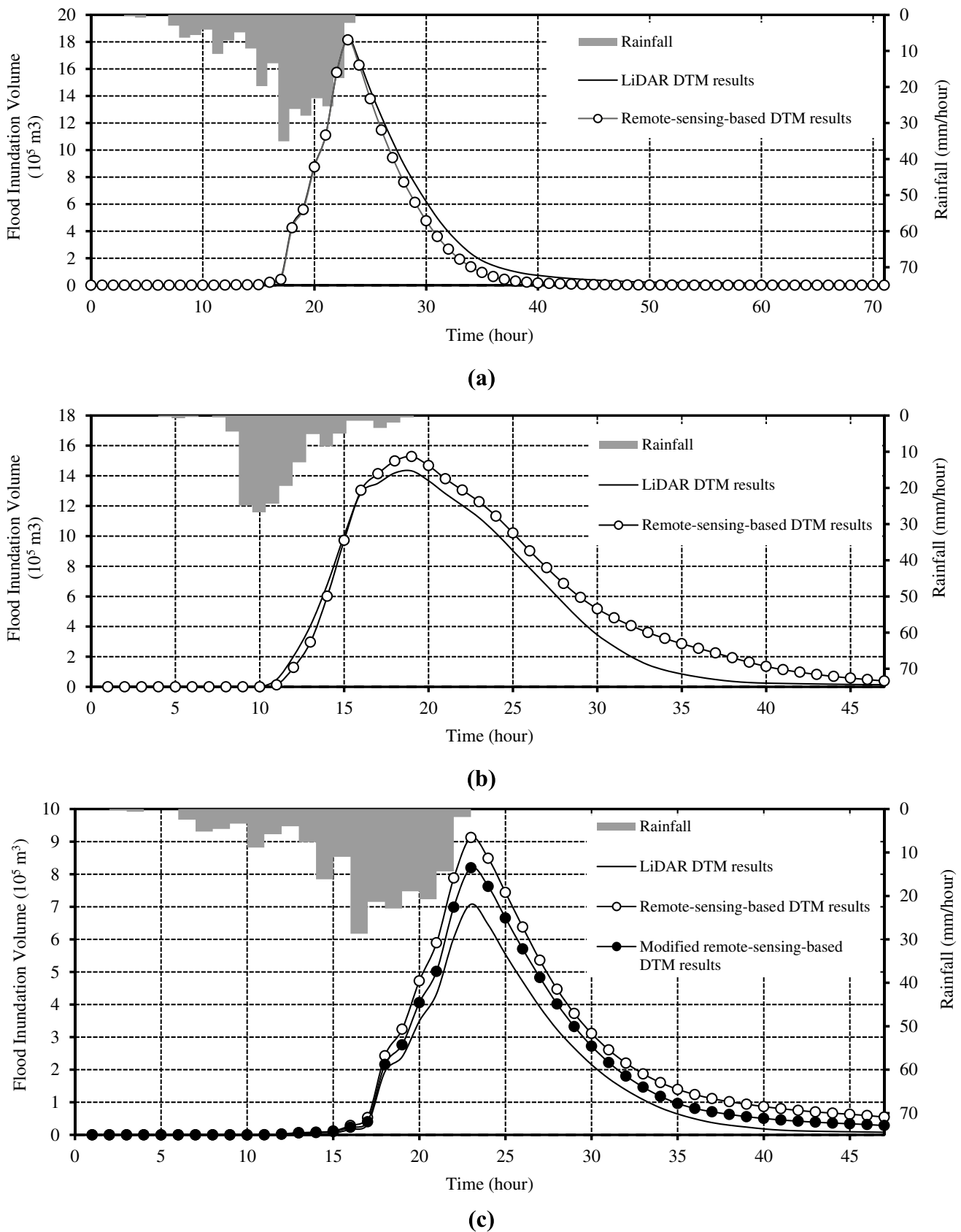
(a)

(b)

(c)

Fig. 5 100-Year return-period flood inundation volume derived using LiDAR elevation and original and modified extracted remote sensing-based DTM elevations at the **a** Kameda, **b** Niitsu, and **c** Shirone watersheds

Table 5 Statistical performance results using originally derived RS-DTM

No.	Watershed	Statistical performance			
		R^2	Rating	NSE	Rating
1	Kameda	0.992	very good	0.986	very good
2	Niitsu	0.975	very good	0.957	very good
3	Shirone	0.991	very good	0.799	good

In addition, flood inundation area based on inundation depth at peak time between LiDAR and remote sensing-based DTM were also compared (Fig. 8). Notably, the assessment based on peak inundation depth for the three areas revealed no significant differences between the approaches, despite the slight disparities.

Discussions of RS-DTM for inland flood modeling

Based on the statistical performance results, RS-DTM is feasible for use in inland flood modeling. However, the original findings revealed a relative shift in elevation compared with the actual topography. As we hypothesized, the establishment of consistent (equally scattered) geodetic height references is crucial for ensuring a standardized base elevation. In the study, the RS-DTM was developed based on a set of nine reference points, of which only three references points were situated within the watersheds. The results showed that even though the RS-DTM had a 95% confidence level, there was distortion in areas far from the reference points, resulting in larger relative errors in the southwestern part of the Shirone watershed.

Thus, we confirmed that the revision of DTM successfully enhanced the correlation in Shirone watershed between flood inundation volumes derived from the LiDAR data and the flood modeling outcomes generated using the RS-DTM. Overall, this approach validated that the non-uniform distribution of height references may be the primary factor contributing to the relative shift.

Furthermore, there were several factors might have contributed to this discrepancy, which could not be addressed. First, the conversion process from DSM to DTM lacked refinement, and the mathematical surface model used remained uniform across the entire DSM/DTM. This is demonstrated by the increased frequency of height differences in the northern region of the Kameda watershed, which corresponds to urban areas, while in the central region, the landscape is predominantly characterized by agricultural fields with fewer disparities in elevation (Fig. 6).

Second, temporal and angular discrepancies in the data acquisition may be problematic. These discrepancies can occur owing to several factors such as lens distortions, image alignment errors, or inaccuracies in camera calibration. The images were not sourced from a single acquisition, particularly for large areas. Variations in data acquisition also affected the incidence angle, which differed between acquisitions. In addition to the influence of tree/building shadows, clouds, and their shadows, water surfaces introduce errors during the DSM extraction.

Finally, issues were potentially acquired through the transformation of the geodetic projection system from global (EGM, 2008) to regional (JPS, 2011). Geodetic map projection systems were employed during the conversion of DSM into DTM. The transformation from a global to a regional system introduces horizontal and vertical differences.

Conclusions and recommendations

In summary, topographic elevations generated by remote sensing approaches were used for reliable flood inundation analysis modeling. In a study of three watersheds in Kameda, Niitsu, and Shirone (Japan), the assessment of DTMs showed that the RS-DTM exhibited high reliability, with R^2 values exceeding 0.93 and RMSE varying between 0.234 and 0.718 m, based on a comparison of topography from the LiDAR.

The volume of flood inundation resulting from the LiDAR and original extracted RS-DTM elevations showed good results—Kameda and Niitsu yielded R^2 and NSE values that exceeded 0.9. On the other hand, despite achieving a 'very good' classification for R^2, the Shirone watershed exhibited a weaker NSE correlation, falling within the 'good' category. Therefore, the topography was adjusted to enhance the correlation between the resulting flood model

Table 6 Modified intercept and coefficient results for topographic revisions

No.	Watershed	Regression analysis formula	Coefficient/slope	Relative slope revision	Intercept/constant	Relative elevation revision
1	Kameda	$y = 1.0005x - 0.0718$	1.0005	–	−0.0718	–
2	Niitsu	$y = 0.9931x + 0.0653$	0.9931	–	+0.0613	–
3	Shirone	$y = 0.9431x - 0.0953$	0.9431	1/0.9431	−0.0953	+0.0953

Fig. 6 Height differences and cross-sectional profile between LiDAR and remote sensing-based DTM
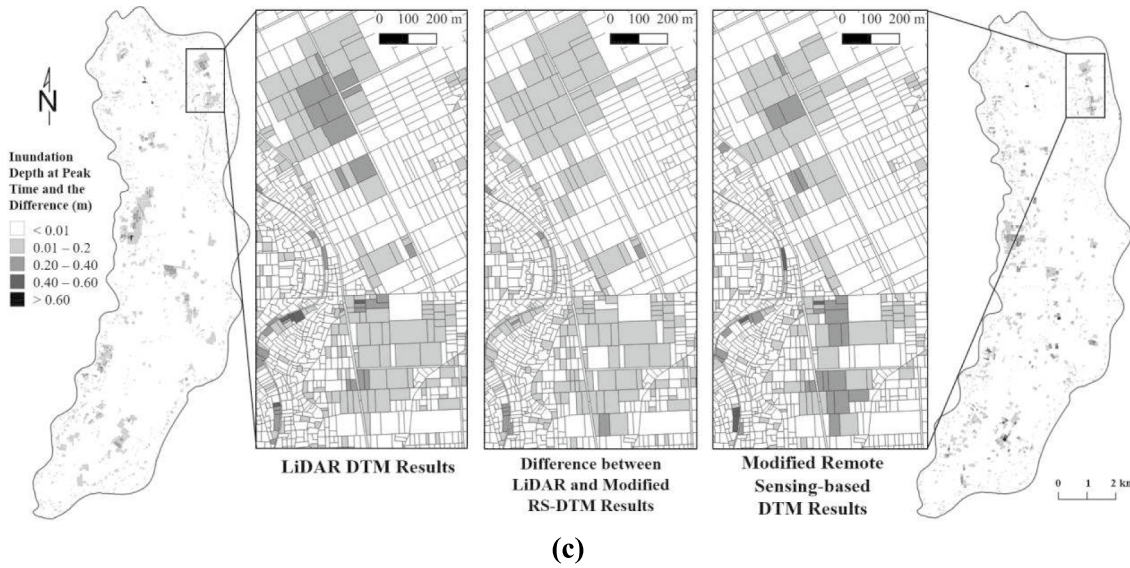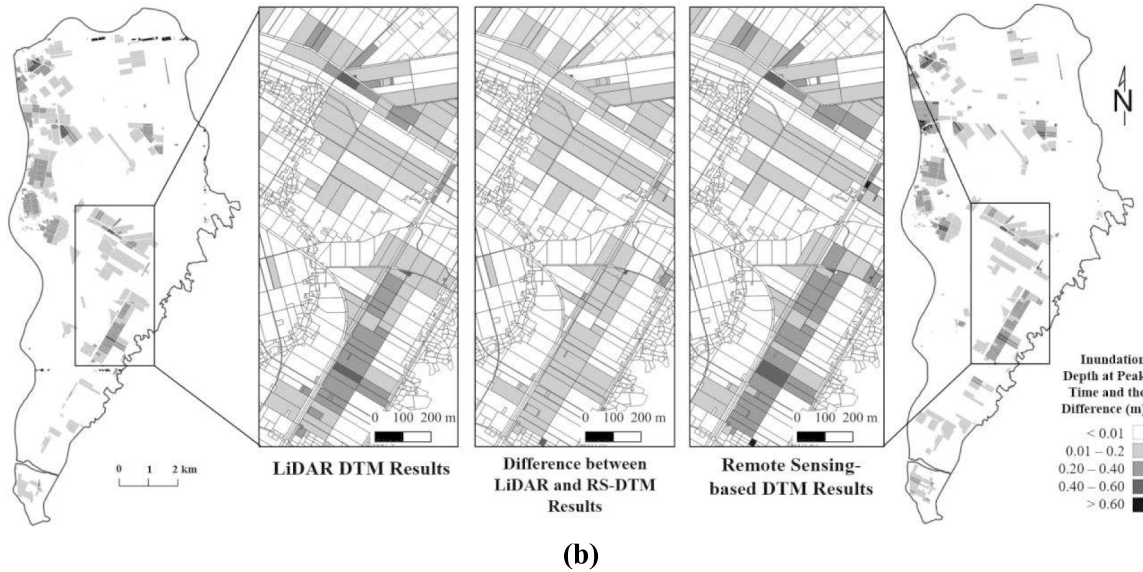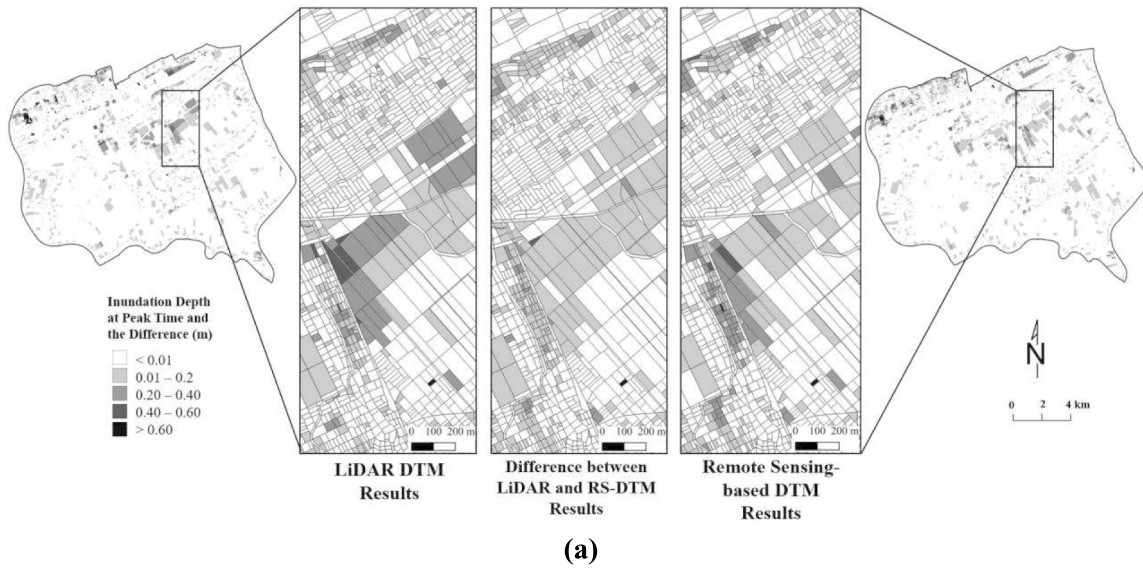
(a)

(b)

(c)
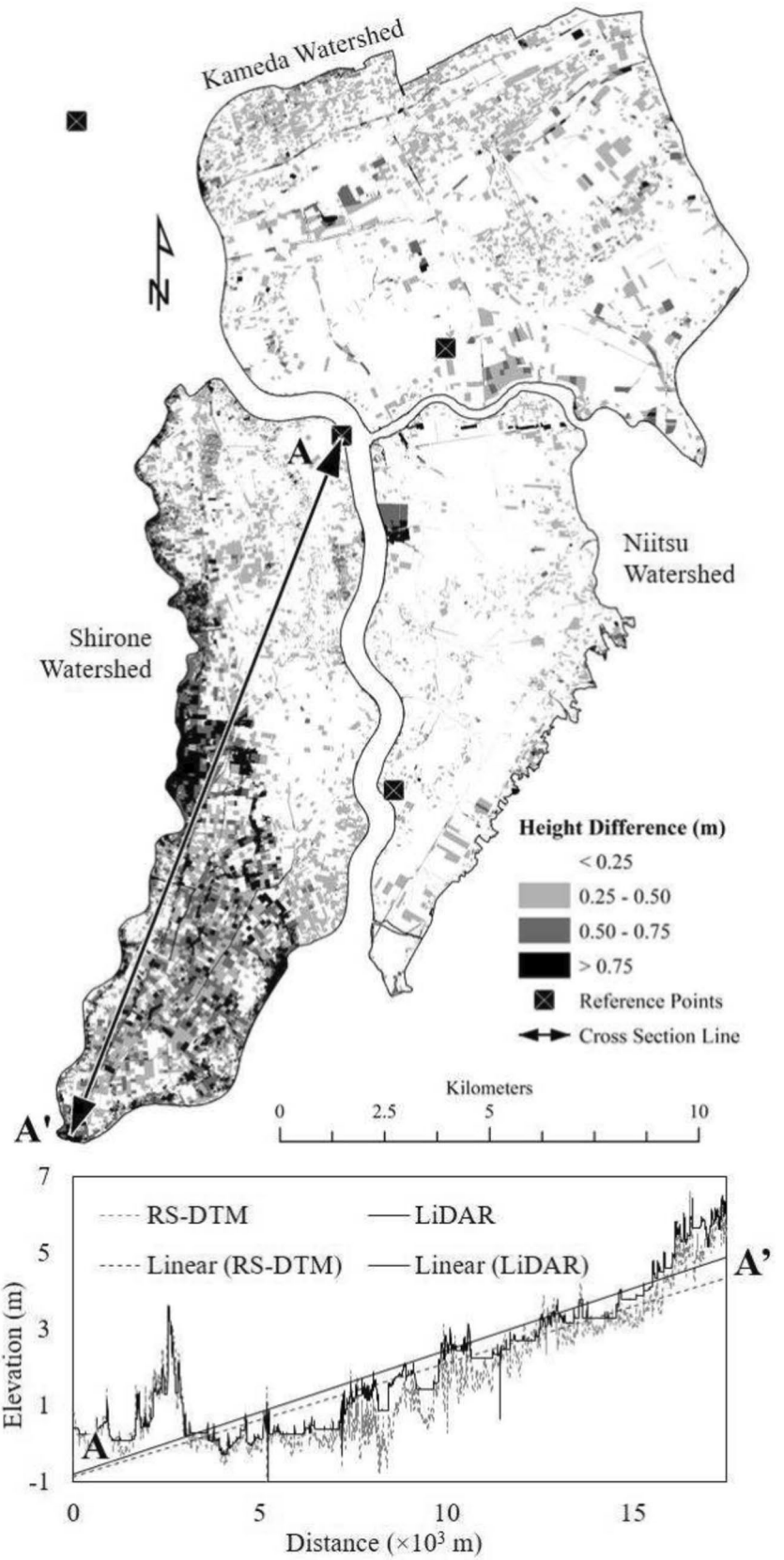
◄**Fig. 7** Visual comparison of flood inundation depth at peak time between LiDAR results, remote sensing-based DTM outputs, and the differences in **a** Kameda, **b** Niitsu, and **c** Shirone

derived from the LiDAR data and RS-DTM. This revision at Shirone watershed successfully improved the correlation,

achieving R^2 results for the three watersheds ranging from 0.975 to 0.997 and NSE values ranging from 0.938 to 0.986 between the resulting flood models based on the LiDAR data and RS-DTM.

Based on the findings of this study, the utilization of geodetic height references holds significance, particularly in

(a)

(b)

(c)
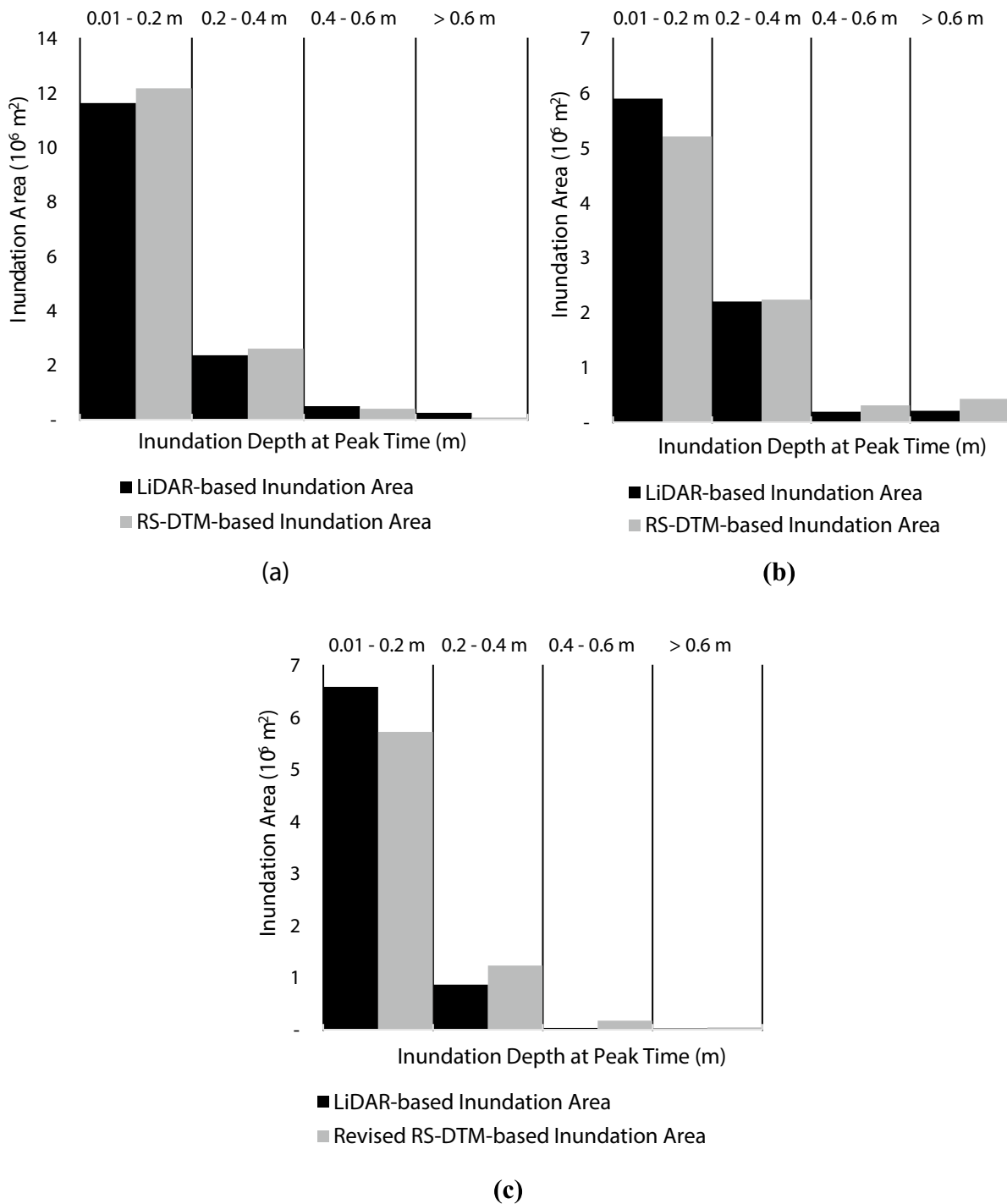
Fig. 8 Inundated area based on inundation depth at peak time between LiDAR and remote sensing-based DTM results in **a** Kameda, **b** Niitsu, and **c** Shirone

ensuring that reference points are evenly distributed across the study site. Unevenly distributed reference points can lead to certain areas of the study site being disproportionately influenced by less accurate interpolated elevations, ultimately causing a relative shift within the study area. Hence, if a sufficient number of height references are unavailable to ensure uniform data coverage within a study site, the utilization of instruments such as static GNSS and electronic total stations, which provide precise positioning and elevation measurements, is feasible. In such scenarios, interpolation can provide satisfactory and representative height references.

In conclusion, the utilization of RS-DTM with uniformly distributed height references in lowland regions offers cost-effective advantages by reducing labor-intensive efforts and eliminating the need for extensive fieldwork. The availability of RS-DTM data reduces reliance on specialized equipment and personnel, streamlines workflow, and reduces financial burden. Moreover, the DTM enables flood modeling studies in flood-prone regions worldwide, including lowland/river delta regions, particularly in developing countries with limited access to high-resolution DTMs.

References

Bruinsma SL, Sánchez-Ortiz N, Olmedo E, Guijarro N (2012) Evaluation of the DTM-2009 thermosphere model for benchmarking purposes. J Space Weather Space Clim 2:A04. https://doi.org/10.1051/swsc/2012005

Burrough PA, McDonnell RA (1998) Principles of geographical information systems. Oxford University Press

Chen H, Liang Q, Liu Y, Xie S (2018) Hydraulic correction method (HCM) to enhance the efficiency of SRTM DEM in flood modeling. J Hydrol 559:56–70. https://doi.org/10.1016/j.jhydrol.2018.01.056

Escobar-Silva EV, Almeida CMd, Silva GBLd, Bursteinas I, Rocha FKLd, de Oliveira CG, Fagundes MR, Paiva RCDd (2023) Assessing the extent of flood-prone areas in a south-American megacity using different high-resolution DTMs. Water 15(6):1127. https://doi.org/10.3390/w15061127

Ettritch G, Hardy A, Bojang L, Cross D, Bunting P, Brewer P (2018) Enhancing digital elevation models for hydraulic modelling using flood frequency detection. Remote Sens Environ 217:506–522. https://doi.org/10.1016/j.rse.2018.08.029

Gamba P, Dell Acqua F, Houshmand B (2002) SRTM data Characterization in urban areas. Int Arch Photogram Remote Sens Spatial Inf Sci 34:55–58

Geospatial Information Authority of Japan (GSI) (2020) The latest DEM data (5-meter mesh) [Data set of Kameda, Niitsu, and Shirone]. Ministry of Land, Infrastructure, Transport and Tourism. https://fgd.gsi.go.jp/download/menu.php.

Geospatial Information Authority of Japan (GSI) (2023) Reference Point Results Browsing Service [Reference points set of Kameda, Niitsu, and Shirone]. Ministry of Land, Infrastructure, Transport and Tourism. https://sokuseikagis1.gsi.go.jp.

Guth P (2003) Geomorphology of DEMs: quality assessment and scale effects. Paper No. 175–2. In Proceedings of GSA, Seattle Annual Meeting, November 2–5, 2003.

Harel O (2009) The estimation of R^2 and adjusted R^2 in incomplete data sets using multiple imputation. J Appl Stat 36(10):1109–1118. https://doi.org/10.1080/02664760802553000

Hengl T, Heuvelink GBM, Rossiter DG (2007) About regression-kriging: from equations to case studies. Comput Geosci 33(10):1301–1315. https://doi.org/10.1016/j.cageo.2007.05.001

Jiang W, Yu J, Wang Q, Yue Q (2022) Understanding the effects of digital elevation model resolution and building treatment for urban flood modelling. J Hydrol: Reg Studies 42:101122. https://doi.org/10.1016/j.ejrh.2022.101122

Julzarika A, Aditya T, Subaryono S, Harintaka H (2021a) The latest DTM using InSAR for dynamics detection of Semangko fault-Indonesia. Geodesy Cartography (vilnius) 47(3):118–130. https://doi.org/10.3846/gac.2021.12621

Julzarika A, Aditya T, Subaryono HH, Dewi RD, Subehi L (2021b) Integration of the latest digital terrain model (DTM) with Synthetic aperture radar (SAR) bathymetry. J Degrad Min Lands Manag 8(3):2759–2768. https://doi.org/10.15243/jdmlm.2021.083.2759

Julzarika A, Harintaka H (2019) Utilization of Sentinel Satellite for Vertical Deformation Monitoring in Semangko Fault-Indonesia. In The 40th Asian Conference on Remote Sensing (ACRS 2019), 1–7. https://a-a-r-s.org/proceeding/ACRS2019/WeA2-3.pdf.

Julzarika A (2021) The Updated DTM Model using ALOS PALSAR/PALSAR-2 and Sentinel-1 Imageries for Dynamic Topography. Dissertation. Universitas Gadjah Mada.

Jurjević L, Gašparović M, Liang X, Balenović I (2021) Assessment of close-range remote sensing methods for dtm estimation in a lowland deciduous forest. Remote Sens 13(11):2063. https://doi.org/10.3390/rs13112063

Kimura N, Kiri H, Kanada S, Kitagawa I, Yoshinaga I, Aiki H (2019) Flood simulations in mid-latitude agricultural land using regional current and future extreme weathers. Water 11(11):2421. https://doi.org/10.3390/w11112421

Lefsky MA, Cohen WB, Parker GG, Harding DJ (2002) Lidar remote sensing for ecosystem studies: lidar, an emerging remote sensing technology that directly measures the three-dimensional distribution of plant canopies, can accurately estimate vegetation structural attributes and should be of particular interest to forest, landscape, and global ecologists. J BioSci 52(1):19–30. https://doi.org/10.1641/0006-3568(2002)052[0019:lrsfes]2.0.co;2

Magruder L, Neuenschwande A, Klotz B (2021) Digital terrain model elevation corrections using space-based imagery and ICESat-2 laser altimetry. Remote Sens Environ 264:112621. https://doi.org/10.1016/j.rse.2021.112621

Meesuk V, Vojinovic Z, Mynett AE, Abdullah AF (2015) Urban flood modelling combining top-view LiDAR data with ground-view SfM observations. Adv Water Resour 75:105–117. https://doi.org/10.1016/j.advwatres.2014.11.008

Merkuryeva G, Merkuryev Y, Sokolov BV, Potryasaev S, Zelentsov VA, Lektauers A (2015) Advanced river flood monitoring, modelling and forecasting. J Comput Sci 10:77–85. https://doi.org/10.1016/j.jocs.2014.10.004

Mesa-Mingorance JL, Ariza-López FJ (2020) Accuracy assessment of digital elevation models (DEMs): a critical review of practices of the past three decades. Remote Sens 12(16):2630. https://doi.org/10.3390/rs12162630

Nash JE, Sutcliffe JV (1970) River flow forecasting through conceptual models: part 1. A discussion of principles. J Hydrol 10(3):282–290. https://doi.org/10.1016/0022-1694(70)90255-6

Néelz S, Pender G, Villanueva I, Wilson M, Wright NG, Bates P, Mason D, Whitlow C (2006) Using remotely sensed data to support flood modelling. In: Proceedings of the Institution of Civil Engineers: Water Management. https://doi.org/10.1680/wama.2006.159.1.35.

Nguyen NB, Nguyen NH, Tran DT, Tran PT, Pham TG, Nguyen TM (2020) Assessing damages of agricultural land due to flooding in a lagoon region based on remote sensing and GIS: case study of the Quang Dien district, Thua Thien Hue province, central Vietnam. J Vietnam Environ 12(2):100–107. https://doi.org/10.13141/jve.vol12.no2.pp100-107

Pavlova AI, Pavlov AV (2018) Analysis of correction methods for digital terrain models based on satellite data. Optoelectron Instr Proc 54:445–450. https://doi.org/10.3103/S8756699018050035

Rau MI, Hidayatulloh MH, Suharnoto Y, Arif C (2021) Evaluation of flood modelling using online visual media: case study of Ciliwung River at Situ Duit Bridge, Bogor City, Indonesia. In IOP Conf Series: Earth Environ Sci 622(1):012041. https://doi.org/10.1088/1755-1315/622/1/012041

Rucci A, Ferretti A, Monti Guarnieri A, Rocca F (2012) Sentinel 1 SAR interferometry applications: the outlook for sub millimeter measurements. Remote Sens Environ 120:156–163. https://doi.org/10.1016/j.rse.2011.09.030

Stock JD, Bellugi D, Dietrich WE, Allen D (2002) Comparison of SRTM topography to USGS and high-resolution laser altimetry topography in steep landscapes: case studies from Oregon and California. In AGU Fall Meeting Abstracts 2002:H21G – H29

Suhadha AG, Julzarika A (2022) Dynamic displacement using DInSAR of Sentinel-1 in Sunda Strait. Trends Sci 19(13):4623. https://doi.org/10.48048/tis.2022.4623

Van Liew MW, Arnold JG, Garbrecht JD (2003) Hydrologic simulation on agricultural watersheds: choosing between two models. Transact ASAE 46(6):1539–1551. https://doi.org/10.13031/2013.15643

Wedajo GK, LiDAR DEM (2017) Data for flood mapping and assessment; opportunities and challenges: a review. J Remote Sens Gis 6:2015–2018. https://doi.org/10.4172/2469-4134.1000211

Wilson JP (2012) Digital terrain modeling. Geomorphology 137(1):107–121. https://doi.org/10.1016/j.geomorph.2011.03.012

Xu K, Fang J, Fang Y, Sun Q, Wu C, Liu M (2021) The importance of digital elevation model selection in flood simulation and a proposed method to reduce DEM errors: a case study in Shanghai. Int J Disaster Risk Sci 12:890–902. https://doi.org/10.1007/s13753-021-00377-z

Yasuda H, Shirato M, Goto C, Yamada T (2003) Development of rapid numerical inundation model for the levee protection activity. Doboku Gakkai Ronbunshu 740:1–17. https://doi.org/10.2208/jscej.2003.740_1

Yoshikawa N, Miyazu S, Yasuda H, Misawa S (2011) Development of inundation analysis model for low-lying agricultural reservoir. Journal of Japan Society of Civil Engineers, Ser. B1 (Hydraulic Engineering), 67(4), I_991–I_996. https://doi.org/10.2208/jscejhe.67.I_991